Magnon Interference Tunneling Spectroscopy as a Probe of 2D Magnetism

Asimpunya Mitra,[1,2] Alberto Corticelli,[3] Pedro Ribeiro,[4,5] and Paul A. McClarty[3]
[1]Department of Physics, Indian Institute of Technology Kharagpur, Kharagpur 721302, India
[2]Department of Physics, University of Toronto, Toronto, Ontario M5S 1A7, Canada
[3]Max Planck Institute for the Physics of Complex Systems, Nöthnitzer Strasse 38, 01187 Dresden, Germany
[4]CeFEMA, Instituto Superior Técnico, Universidade de Lisboa, Avenue Rovisco Pais, 1049-001 Lisboa, Portugal
[5]Beijing Computational Science Research Center, Beijing 100084, China

(Received 25 November 2021; revised 28 October 2022; accepted 9 January 2023; published 10 February 2023)

Probing two-dimensional single-layer quantum magnets remains a significant challenge. In this Letter, we propose exploiting tunneling spectroscopy in the presence of magnetic impurities to obtain information about the magnon dispersion relations in analogy to quasiparticle interference in nonmagnetic materials. We show that this technique can be used to establish the dispersion relations even for frustrated magnets, where the presence of an impurity generally leads to a nontrivial spin texture. Finally, we consider the problem of establishing Chern magnon bands in 2D magnets showing how tunable impurities allow one to probe the nature of the surface states.

DOI: 10.1103/PhysRevLett.130.066701

One of the most exciting recent developments in magnetism is the fabrication of truly 2D magnets on nonmagnetic substrates, opening up the possibility of both engineering and exploring novel exotic and interesting low-dimensional collective phenomena. Notable examples include twisted bilayer graphene, which under certain circumstances becomes insulating with spontaneous ferromagnetism and Chern bands [1–3], and the chromium trihalides that are insulating honeycomb ferromagnets [4–7]. With advances in materials science, there appear to be excellent prospects for the proliferation of engineered few-layer magnetic materials with many different kinds of magnetic ions arranged on various lattices and substrates.

A pressing challenge in this area is to develop new techniques to probe such systems. Examples include magnetometry using nitrogen vacancy centers—which has potential as a probe of magnetic structures and low energy magnetic dynamics [8], mesoscopic Hall currents for the uniform susceptibility [9], and electron magnetic chiral dichroism to probe magnetic structures at the atomic scale [10]. In this Letter, we propose using impurity-induced magnon interference tunneling spectroscopy to probe the magnetic properties of 2D materials, as a solution to the long-standing problem of characterizing magnetism in these materials.

Scanning tunneling microscopy (STM) is a well-established technique to probe local charge and spin properties. In recent landmark work, the viability of STM to observe magnetic excitations has also been successfully demonstrated [11–13]. In many electronic materials, it is possible to infer nonlocal charge properties by measuring the spatial response to isolated impurities. This technique, called quasiparticle interference (QPI), has also been used to obtain crucial information about electronic correlations [14–16].

Here, we show that the magnetic analog of QPI—magnon interference tunneling spectroscopy—can be used to study isolated magnetic layers on conducting substrates through the magnetic scattering of tunneling electrons by impurities. In particular, this technique can provide momentum- and energy-resolved information about magnons in ordered two-dimensional magnets.

The Letter is organized as follows. We first outline the proposed experimental configuration and give an expression for the tunneling conductance due to inelastic scattering from magnons together with an explanation of the underlying assumptions.

We then turn to the modeling of an impurity in an otherwise undisturbed 2D lattice of magnetic ions and study its STM interference pattern in real and momentum space. We illustrate how interference effects can be used to infer magnon dispersion relations in various cases, including (i) single-band unfrustrated magnets, (ii) multiple-band unfrustrated magnets with touching points, and (iii) frustrated magnets with multiple bands, where the magnetic ground state itself is destabilized in the vicinity of the impurity [17]. Finally, we show the potential of engineered impurity scattering to probe properties of Chern magnon bands.

Tunneling of electrons through a magnetic layer.—Before considering the effects of impurities, we consider

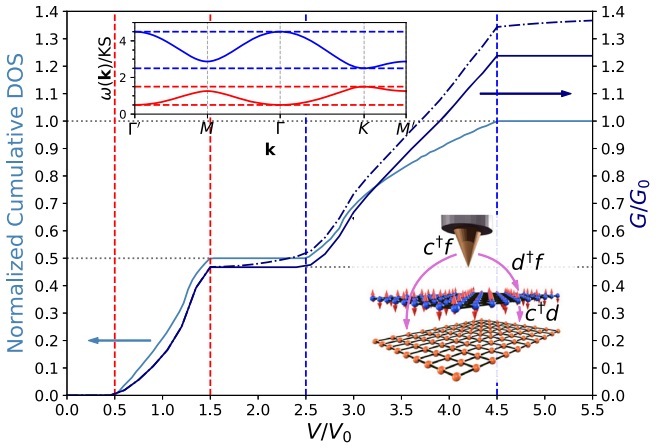

FIG. 1. Normalized cumulative density of states (DOS) (left axis) and normalized inelastic tunneling conductance G/G_0 (right axis) plotted as a function of bias voltage V for the Kitaev-Heisenberg model with $\theta = \pi/2$ and $h = 4.5$ and the STM with $a/\lambda = 1$. The dashed line shows the inelastic conductance with both single- and two-magnon continuum contributions taken into account. The top inset shows the dispersion relations along the indicated high symmetry directions in reciprocal space; dashed lines indicate the band edges. The bottom inset shows a schematic of a STM setup. Arrows show the various tunneling processes.

the setup shown in Fig. 1 (lower inset) featuring a STM tip over an insulating magnetic layer mounted on a conducting substrate. The tip is positioned laterally at $\boldsymbol{r}_T$ with vertical distance d_1 just above a magnetic layer and vertical distance d_2 between the layer and the substrate.

We are interested in the tunneling conductance originating from inelastic scattering from localized moments when a bias voltage V is applied between the tip and the substrate. Similar situations were considered in Refs. [18–25].

Hybridization between local moments and conduction electrons can alter the nature of the magnetic layer in several ways. For example, it may destroy the insulating nature of the monolayer. We focus on cases where the charge gap in the insulating layer is much larger than the magnetic energy scale. Even where the layer is metallic, there may be magnetic order in the ground state, though analysis of this scenario is beyond the scope of this Letter. When the hybridization is perturbative in nature, the magnetic couplings in the layer will depend, in general, on the presence of the proximate conductor—for example, through Ruderman-Kittel-Kasuya-Yosida couplings that can be understood within our approach. The effects of the substrate may be more severe: for example, under different conditions the layer may undergo charge disproportionation. Our calculation can, in principle, be adapted to the case where magnetic order coexists with charge ordering. For illustration, we consider here various exchange models and evaluate the dynamical structure factor (DSF) within spin wave theory [26].

We further consider the tip and the substrate to be wideband metals with a constant density of states. This approximation is appropriate in a typical situation where the magnetic energy scales are small as compared to electronic scales.

Under these assumptions, the leading contribution to the tunneling conductance may be computed within a strong coupling perturbation theory and within linear response [26]. The tunneling conductance is

$$G(V) = G_0 \sum_{\boldsymbol{r}_{Ia}\boldsymbol{r}'_{Ib}} e^{-\frac{2}{\lambda}(|\boldsymbol{r}_{Ia}-\boldsymbol{r}_T|+|\boldsymbol{r}'_{Ib}-\boldsymbol{r}_T|)} \int_0^{\mathrm{eV}} d\omega \sum_{\alpha} \tilde{S}^{\alpha\alpha}_{\boldsymbol{r}_{Ia}\boldsymbol{r}'_{Ib}}(\omega), \quad (1)$$

where $\sum_\alpha \tilde{S}^{\alpha\alpha}_{\boldsymbol{r}_{Ia}\boldsymbol{r}'_{Ib}}(\omega) = (1/2\pi)\int d\mathbf{k} \sum_\alpha S^{\alpha\alpha}_{ab}(\mathbf{k},\omega) \times e^{-i\mathbf{k}\cdot(\boldsymbol{r}_{Ia}-\boldsymbol{r}'_{Ib})}$. $\boldsymbol{r}_I$, $\boldsymbol{r}'_I$ are the primitive lattice sites on the magnetic layer; $\boldsymbol{r}_a$, $\boldsymbol{r}_b$ denote basis vectors for the sublattices and $\boldsymbol{r}_{Ia} = \boldsymbol{r}_I + \boldsymbol{r}_a$. $S^{\alpha\alpha}_{ab}(\mathbf{k},\omega)$ is the α spin component of the momentum-energy-dependent DSF [26]. G_0 is a number that is proportional to $\exp[-2(d_1+d_2)/d]$, where d and λ are, respectively, vertical and lateral tunneling lengths assumed to be the same for tunneling from the magnetic layer to both the substrate and to the tip. Within linear spin wave theory, the DSF has a single-magnon contribution coming from the transverse spin components within the local quantization frame, while a two-magnon contribution arises from the longitudinal component [26,28]. In the above discussion, we have focused, for simplicity, on the case where the STM tip is unpolarized. When, instead, it is spin polarized, one gains additional information about the components of the dynamical structure factor as discussed further in the Supplemental Material [26] (Sec. I.2).

Figure 1 shows the conductance and cumulative density of states as a function of voltage for the honeycomb lattice with Kitaev exchange couplings and with moments polarized perpendicular to the plane by an external magnetic field [29]. This model has two dispersive magnon bands at finite energy, as shown in the upper inset of Fig. 1. The inelastic component of the conductance is zero up to the voltage corresponding to the base of the lowest magnon band. Then, the tunneling conductance increases as more scattering channels become available at higher energies. The band gap is visible as a plateau in the conductance. The tunneling conductance plateaus again above the maximum energy of the highest magnon band. In short, the on-site tunneling supplies information about the magnon cumulative density of states and reveals the presence of band gaps. Further examples are discussed in the Supplemental Material [26] (Fig. S2).

As one is usually interested more in the density of states than in the cumulative density of states, it is convenient to consider the *differential* conductance $G(V+\delta V) - G(V)$ for different on-site positions where δV is a current averaging window.

The calculations discussed so far are based on single-magnon inelastic scattering. However, the spin correlator contains contributions from multimagnon scattering events. In the Supplemental Material [26], we examine the role of two-magnon scattering that, to leading order in $1/S$, comes from the S^z operator in the quantization frame. The two-magnon states form a continuum in momentum and energy leading to further scattering channels that increase the conductance (Fig. 1). This contribution can, in principle, obscure the presence of band gaps in the single-magnon band structure [26].

The method is inherently energy resolution limited, as the narrower the energy window, the longer averaging times must be to overcome the temperature varying current noise. A rough benchmark is an $O(1)$ meV resolution at 4.2 K [30]. Recent experiments on bilayer CrI_3 [11] at 300 mK, where shot noise is expected to be the principal contribution to current fluctuations, reveals that a sizable inelastic tunneling signal can be obtained that is plausibly attributable to magnons. Since $O(10–100)$ meV magnetic energy scales are not uncommon, one may expect to resolve details of the local magnetic density of states in many 2D magnetic materials.

Impurity scattering and QPI for magnons.—In conventional QPI, the breaking of translational invariance in the vicinity of spatial disorder leads to a tunneling conductance with a spatial dependence that is tied to the electronic band structure. Here, in order to uncover more detailed information about the magnetic excitations in 2D magnets, we propose exploring the inelastic tunneling conductance in the vicinity of on-site disorder in the magnet. In the following, we consider the case where single vacancies are present in an otherwise pristine lattice of magnetic ions, though similar considerations hold for any type of pointlike disorder, such as interstitial magnetic ions. We distinguish between two main cases: unfrustrated and frustrated magnetic interactions. An example of the former is the square lattice antiferromagnet. Such models have the feature that the magnetic ground state is stable to the presence of impurities. In contrast, magnetic frustration destabilizes the magnetic structure around impurity sites.

Square lattice antiferromagnet.—We consider first the unfrustrated case and, in particular, the Néel ordered square lattice Heisenberg antiferromagnet. This model has linearly dispersing Goldstone modes at the zone center and zone corners. Because the moment orientation is undisturbed when a single magnetic site is removed, one may obtain the local dynamical structure factor (LDSF) exactly. This can be done by writing the linear spin wave Hamiltonian as $H = H_0 + V$, where H_0 is the spin wave Hamiltonian for clean system and V is the impurity contribution. The single-particle Matsubara Green's functions, in terms of the Holstein-Primakoff bosons for the full problem $\boldsymbol{\mathcal{G}}(i\omega_n)$, satisfy a Dyson equation $\boldsymbol{\mathcal{G}}(i\omega_n) = \boldsymbol{\mathcal{G}}_0(i\omega_n) + \boldsymbol{\mathcal{G}}(i\omega_n)\boldsymbol{V}_0(i\omega_n)$ that can be solved numerically exactly based on analytical Green's functions $\boldsymbol{\mathcal{G}}_0(i\omega_n)$ for the spin wave theory in the absence of impurities [26]. In the above formulas, we use bold to indicate that the Green's functions and potential $\boldsymbol{V}$ are matrix value with indices referring to lattice sites and number conserving and nonconserving terms in the Holstein-Primakoff bosons (see Supplemental Material [26] for further details). With $\boldsymbol{\mathcal{G}}(i\omega_n)$, one may evaluate the conductance in Eq. (1) to leading order because, for the problems we shall consider using this approach, $\tilde{S}^{xx}_{\mathbf{r}_a\mathbf{r}_a}(\omega) = \tilde{S}^{yy}_{\mathbf{r}_a\mathbf{r}_a}(\omega) = -(1/\pi)\mathrm{Im}[\mathcal{G}_{\mathrm{ret}}(\omega)]_{\mathbf{r}_a\mathbf{r}_a}$, where $\boldsymbol{\mathcal{G}}_{\mathrm{ret}}(\omega)$ is the retarded single-particle Green's function in terms of Holstein-Primakoff bosons [26]. Further assuming $\lambda/a \ll 1$, the differential conductance $\partial_V G(V)$ becomes proportional to the LDSF.

In Fig. 2 (left panel), the LDSF is plotted at fixed energy $\omega/4JS = 0.875$, where $4JS$ is the magnon bandwidth. The ripples extending out from the impurity correspond to the momentum space pattern in the middle panel. Further energy slices are shown in the Supplemental Material [26]. In real space, as the energy increases from zero, roughly circular waves emanate from the impurity with decreasing wavelength as the voltage increases [see Figs. S5(a) and S5(b) in the Supplemental Material [26]]. These have a direct interpretation in terms of the linearly dispersing Goldstone mode. In the corresponding Fourier transformed pattern, the differential conductance has rings around the (0,0) and (π,π) points with radius $k_{\max} = 2\omega/v$, where v is the velocity of the mode. At higher energies, the magnon band flattens out and more scattering channels open up [26] with the result that (i) the real space pattern evolves from circular waves at low energies to a C_4 symmetric pattern at higher energies and (ii) the Fourier transformed pattern acquires much richer features at higher energies than at lower energies. Nevertheless, these patterns have a direct interpretation in terms of the joint density of states $\rho(\boldsymbol{q},\omega) = \int d^2\boldsymbol{k}/(2\pi)^2\delta(\omega - \epsilon_{\boldsymbol{q}+\boldsymbol{k}})\delta(\omega - \epsilon_{\boldsymbol{k}})$ plotted in the rightmost panel. The resemblance between the Fourier transform of the constant energy local Green's functions and the joint density of states (JDOS) holds for all energies [26], highlighting the importance of the scattering of two magnons on a constant energy surface $\epsilon_{\boldsymbol{k}} = \epsilon_{\boldsymbol{k}+\boldsymbol{q}}$ [26]. The band structure can, in principle, be inferred from experimental data by parametrizing the joint density of states.

Honeycomb lattice ferromagnet.—Exact calculations of this kind can also be carried out for the two-band honeycomb lattice ferromagnet. In this model, the two bands are connected by Dirac points at K and K' points. Results are shown in the Supplemental Material [26].

QPI with magnetic frustration.—As a final example, we carry out a full calculation of the tunneling conductance on a finite periodic slab for the Kitaev-Heisenberg model [with $\theta = (\pi/2)$] in a magnetic field. Because the model is

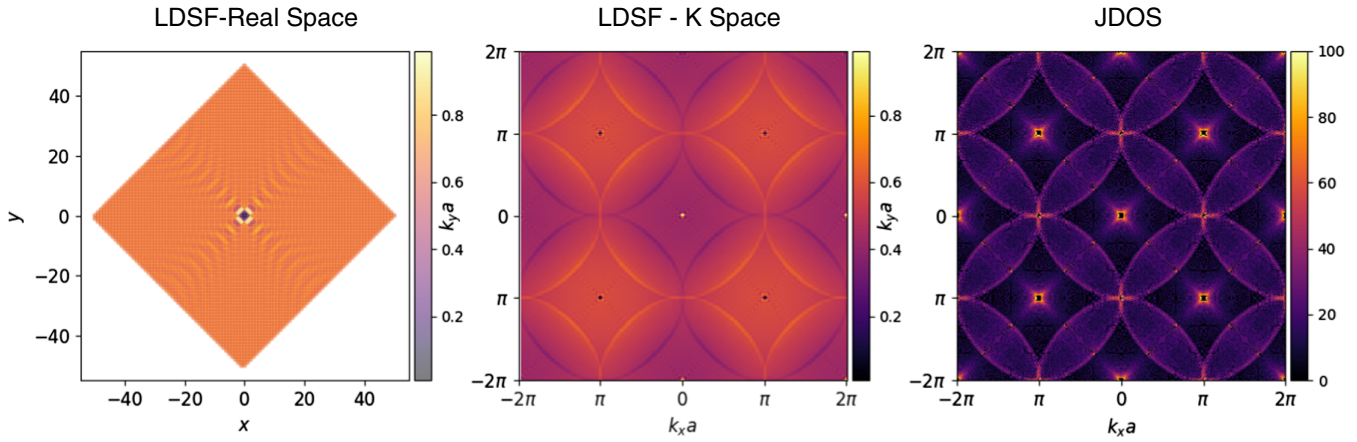

FIG. 2. Effect of a single impurity on the square lattice antiferromagnet at energy $\omega/4JS = 0.875$. Left: the local dynamical structure factor on each site at fixed energy for a $2 \times 50 \times 50$ site slab computed using the T matrix approach. This is proportional to the differential tunneling conductance at fixed voltage in the limit where tunneling can only occur directly to the site beneath the tip. Middle: the Fourier transformed real space pattern. For comparison, we show the joint density of states (right). In the latter plot, for clarity, intensity has been truncated at the zone centers.

frustrated, the presence of an impurity destabilizes the polarized state locally. The ground state texture is one where the moments acquire transverse components that wind around the impurity. The sense of the winding depends on the distance from the impurity and the decay length scale of the texture is related to the inverse magnon gap that can be controlled by a uniform magnetic field. Despite the destabilization of the ground state and finite size effects, the differential tunneling conductance remains in close correspondence with the joint density of states computed from the bulk band structure (see Fig. 3 [26]).

Topological magnon bands.—The Kitaev-Heisenberg model on the honeycomb lattice in the polarized phase has two magnon bands carrying Chern number ± 1 [29,31,32]. Nontrivial band topology of this type implies the presence of chiral magnon edge states. Detecting these edge states is a challenge for experiment because the modes are microscopic—in the sense of an atomically small length scale binding them to the edge—and also because the modes carry no charge and have energy scales significantly below electronic energy scales.

Edge modes are detectable, in principle, as an in-gap contribution to the differential conductance when the tip is positioned at the edge [24], although there may be contamination from magnon continua or bound states. Since the system is translationally invariant parallel to a straight edge, the contribution to the tunneling coming from the edge modes is uniform in that direction. An important question is whether tunneling spectroscopy assisted by impurity scattering can be used to establish the chirality of in-gap modes or that they are topologically protected.

We return to the situation where a vacancy is present in the bulk focusing now on the in-gap region. One may loosely view the vacancy as a hole carrying protected chiral edge states that is shrunk down to atomic proportions. In this limit, the edge states on facing surfaces interact but, instead of destroying the edge modes completely, bound impurity states remain within the bulk gap [Fig. 4(d)]. Such localized in-gap states appear as jumps in the conductance at discrete in-gap voltages when the tip is placed close to the impurity. The presence of such bound states has been argued to be a diagnostic of topological bands, at least when the hopping amplitudes are spatially homogeneous [33,34].

We now consider the QPI pattern found from the tunneling conductance around an impurity for different impurity positions with respect to a boundary. As discussed above, the QPI pattern in momentum space roughly reflects the joint density of states computed from the band structure in the translationally invariant system apart from the presence of the in-gap impurity bound states.

Inspection of the spectrum of the model with impurity close to, but not at, the boundary in a slab calculation reveals that the nearly flat bound impurity modes hybridize with the edge modes leading to avoided crossings over

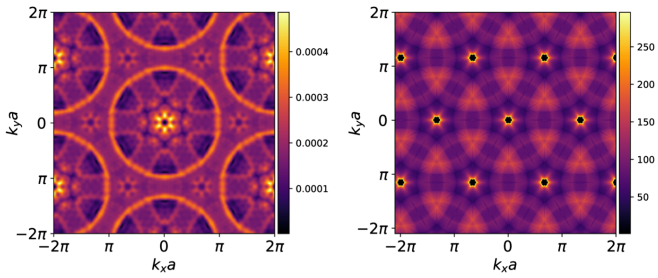

FIG. 3. Magnon QPI results for the spin polarized Kitaev honeycomb model with a single vacancy and $\omega/KS = 1.6$. Left: the Fourier transform of the differential conductance, computed with $\delta V = 0.1$, on the periodic 21×21 slab. Right: the joint density of states. The bands extend from 1.0 to 5.0 in these units.

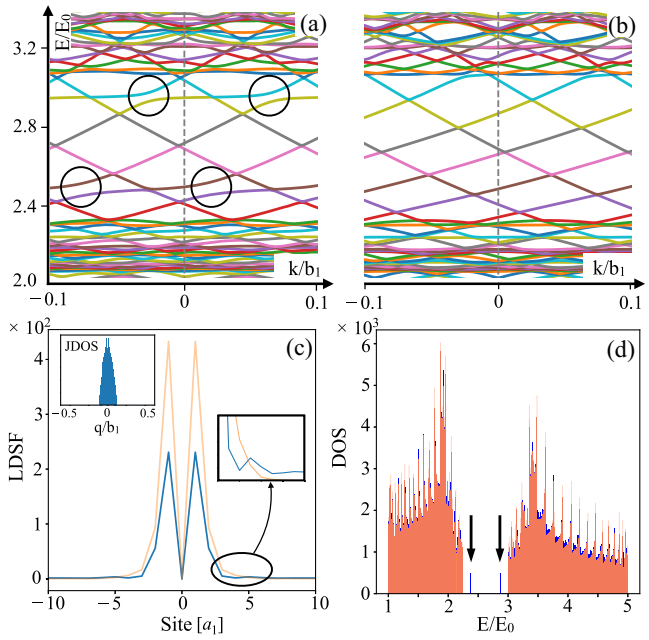

FIG. 4. Calculations for honeycomb Kitaev-Heisenberg model with $\theta = \pi/2$ and magnetic field $h = 5$ perpendicular to the honeycomb plane. (a) Hybridized in-gap magnon states in the presence of a defect in an intermediate position close to the edge (full band dispersion in the Supplemental Material [26]). (b) Renormalized states for a defect at the edge. (c) Local dynamical structure factor for a case with a defect in the bulk (orange) and for a defect hybridizing with the boundary states (blue). The enlargement shows the interference fringe and the inset shows the JDOS. The sites are in units of primitive lattice a_1 along the periodic direction, centered in the defect. (d) DOS for the bulk without defect (pink) and with a defect in the bulk (blue). The two arrows highlight the localized bound states in the gap.

narrow energy ranges [Fig. 4(a)]. This leads to the following picture for the tunneling conductance as the voltage is swept through the in-gap region. For Chern bands supporting a single chiral edge mode, the joint density of states has a single peak at $\boldsymbol{q} = 0$, so one should expect a spatially uniform, or trivial, QPI pattern in real space around an impurity except close to the hybridization energies, even though there are tunneling contributions originating from the edge modes. Over the narrow energy window where hybridization occurs, scattering is possible between the admixed impurity and edge state modes leading to a broadening in the joint density of states that may be observed as a long wavelength spatial modulation in the conductance parallel to the edge [Fig. 4(c)]. Altogether, this provides evidence for the chirality of the edge modes.

If the vacancy lies directly at the boundary, thereby locally roughening the edge, the topological nature of the bands implies that chiral surface states must be present. The principal difference between the case with and without the impurity is that the velocity of the chiral modes is renormalized [Fig. 4(b)]. The robustness of the edge modes to the presence of disorder constitutes further evidence that the boundary modes are protected by the bulk topology.

Summary and outlook.—In this Letter, we have proposed a method to probe 2D magnets mounted onto conducting substrates using a variant of QPI from quenched disorder through the inelastic scattering of tunneling electrons from magnons. We have shown that this method has the potential to provide detailed energy- and momentum-resolved information about the magnon spectrum that can be used to understand the material microscopically. It also allows one, in principle, to probe interfacial magnetism in unprecedented detail, including the dispersion relations of topological magnon surface states. In addition, magnon QPI could perhaps be used in tandem with higher energy probes such as angle-resolved photoemission spectroscopy to understand better the interplay of surface magnetism and electronic structure [35]. Ultimately, the power of the approach discussed here will have to be settled in the laboratory and we hope that this Letter will help inspire the first magnon QPI experiments.

We thank Jeff Rau and Masafumi Udagawa for useful discussions. A. M. acknowledges the support of the KVPY fellowship from DST, Government of India. A. C. and P. M. acknowledge the Deutsche Forschungsgemeinschaft (DFG) Grant No. SFB 1143. P. R. acknowledges support by FCT through Grant No. UID/CTM/04540/2019.

[1] Y. Cao, V. Fatemi, A. Demir, S. Fang, S. L. Tomarken, J. Y. Luo, J. D. Sanchez-Yamagishi, K. Watanabe, T. Taniguchi, E. Kaxiras, R. C. Ashoori, and P. Jarillo-Herrero, Correlated insulator behaviour at half-filling in magic-angle graphene superlattices, Nature (London) **556**, 80 (2018).

[2] A. L. Sharpe, E. J. Fox, A. W. Barnard, J. Finney, K. Watanabe, T. Taniguchi, M. A. Kastner, and D. Goldhaber-Gordon, Emergent ferromagnetism near three-quarters filling in twisted bilayer graphene, Science **365**, 605 (2019).

[3] M. Serlin, C. L. Tschirhart, H. Polshyn, Y. Zhang, J. Zhu, K. Watanabe, T. Taniguchi, L. Balents, and A. F. Young, Intrinsic quantized anomalous Hall effect in a moiré heterostructure, Science **367**, 900 (2020).

[4] B. Huang, G. Clark, E. Navarro-Moratalla, D. R. Klein, R. Cheng, K. L. Seyler, D. Zhong, E. Schmidgall, M. A. McGuire, D. H. Cobden *et al.*, Layer-dependent ferromagnetism in a van der Waals crystal down to the monolayer limit, Nature (London) **546**, 270 (2017).

[5] K. S. Burch, D. Mandrus, and J.-G. Park, Magnetism in two-dimensional van der Waals materials, Nature (London) **563**, 47 (2018).

[6] X. Cai, T. Song, N. P. Wilson, G. Clark, M. He, X. Zhang, T. Taniguchi, K. Watanabe, W. Yao, D. Xiao, M. A. McGuire, D. H. Cobden, and X. Xu, Atomically thin $CrCl_3$: An in-plane layered antiferromagnetic insulator, Nano Lett. **19**, 3993 (2019).

[7] M. Gibertini, M. Koperski, A. F. Morpurgo, and K. S. Novoselov, Magnetic 2D materials and heterostructures, Nat. Nanotechnol. **14**, 408 (2019).

[8] F. Casola, T. van der Sar, and A. Yacoby, Probing condensed matter physics with magnetometry based on nitrogen-vacancy centres in diamond, Nat. Rev. Mater. **3**, 17088 (2018).

[9] M. Kim, P. Kumaravadivel, J. Birkbeck, W. Kuang, S. G. Xu, D. G. Hopkinson, J. Knolle, P. A. McClarty, A. I. Berdyugin, M. Ben Shalom, R. V. Gorbachev, S. J. Haigh, S. Liu, J. H. Edgar, K. S. Novoselov, I. V. Grigorieva, and A. K. Geim, Micromagnetometry of two-dimensional ferromagnets, National electronics review **2**, 457 (2019).

[10] D. Song and R. E. Dunin-Borkowski, Three-Dimensional Measurement of Magnetic Moment Vectors Using Electron Magnetic Chiral Dichroism at Atomic Scale, Phys. Rev. Lett. **127**, 087202 (2021).

[11] D. R. Klein, D. MacNeill, J. L. Lado, D. Soriano, E. Navarro-Moratalla, K. Watanabe, T. Taniguchi, S. Manni, P. Canfield, J. Fernández-Rossier *et al.*, Probing magnetism in 2D van der Waals crystalline insulators via electron tunneling, Science **360**, 1218 (2018).

[12] D. Ghazaryan, M. T. Greenaway, Z. Wang, V. H. Guarochico-Moreira, I. J. Vera-Marun, J. Yin, Y. Liao, S. V. Morozov, O. Kristanovski, A. I. Lichtenstein *et al.*, Magnon-assisted tunnelling in van der Waals heterostructures based on $CrBr_3$, National electronics review **1**, 344 (2018).

[13] W. Ruan *et al.*, Evidence for quantum spin liquid behaviour in single-layer 1T-$TaSe_2$ from scanning tunnelling microscopy, Nat. Phys. **17**, 1154 (2021).

[14] E. W. Hudson, S. H. Pan, A. K. Gupta, K. W. Ng, and J. C. Davis, Atomic-scale quasi-particle scattering resonances in $Bi_2Sr_2CaCu_2O_{8+\delta}$, Science **285**, 88 (1999).

[15] A. Yazdani, C. M. Howald, C. P. Lutz, A. Kapitulnik, and D. M. Eigler, Impurity-Induced Bound Excitations on the Surface of $Bi_2Sr_2CaCu_2O_8$, Phys. Rev. Lett. **83**, 176 (1999).

[16] A. V. Balatsky, I. Vekhter, and J.-X. Zhu, Impurity-induced states in conventional and unconventional superconductors, Rev. Mod. Phys. **78**, 373 (2006).

[17] J. Villain, Insulating spin glasses, Z. Phys. B **33**, 31 (1979).

[18] J. Appelbaum, "$s-d$" Exchange Model of Zero-Bias Tunneling Anomalies, Phys. Rev. Lett. **17**, 91 (1966).

[19] P. W. Anderson, Localized Magnetic States and Fermi-Surface Anomalies in Tunneling, Phys. Rev. Lett. **17**, 95 (1966).

[20] M. Pustilnik and L. I. Glazman, Kondo Effect in Real Quantum Dots, Phys. Rev. Lett. **87**, 216601 (2001).

[21] J. R. Schrieffer and P. A. Wolff, Relation between the Anderson and Kondo Hamiltonians, Phys. Rev. **149**, 491 (1966).

[22] M. Maltseva, M. Dzero, and P. Coleman, Electron Cotunneling into a Kondo Lattice, Phys. Rev. Lett. **103**, 206402 (2009).

[23] J. Fransson, O. Eriksson, and A. V. Balatsky, Theory of spin-polarized scanning tunneling microscopy applied to local spins, Phys. Rev. B **81**, 115454 (2010).

[24] J. Feldmeier, W. Natori, M. Knap, and J. Knolle, Local probes for charge-neutral edge states in two-dimensional quantum magnets, Phys. Rev. B **102**, 134423 (2020).

[25] M. Udagawa, S. Takayoshi, and T. Oka, Scanning Tunneling Microscopy as a Single Majorana Detector of Kitaev's Chiral Spin Liquid, Phys. Rev. Lett. **126**, 127201 (2021).

[26] See Supplemental Material at http://link.aps.org/supplemental/10.1103/PhysRevLett.130.066701 for further details of tunneling and spin wave calculations, additional quasiparticle interference plots and material about topological surface states, which includes Ref. [27].

[27] T. Holstein and H. Primakoff, Field dependence of the intrinsic domain magnetization of a ferromagnet, Phys. Rev. **58**, 1098 (1940).

[28] G. D. Mahan, *Many-Particle Systems* (Princeton University Press, Princeton, NJ, 2008).

[29] P. A. McClarty, X.-Y. Dong, M. Gohlke, J. G. Rau, F. Pollmann, R. Moessner, and K. Penc, Topological magnons in Kitaev magnets at high fields, Phys. Rev. B **98**, 060404(R) (2018).

[30] J. Hoffman, A search for alternative electronic order in the high temperature superconductor $Bi_2Sr_2CaCu_2O_{8+x}$ by scanning tunneling microscopy, Ph.D. thesis, University of California Berkeley, 2003.

[31] D. G. Joshi, Topological excitations in the ferromagnetic Kitaev-Heisenberg model, Phys. Rev. B **98**, 060405(R) (2018).

[32] P. McClarty, Topological magnons: A review, Annu. Rev. Condens. Matter Phys. **13**, 171 (2022).

[33] R.-J. Slager, L. Rademaker, J. Zaanen, and L. Balents, Impurity-bound states and Green's function zeros as local signatures of topology, Phys. Rev. B **92**, 085126 (2015).

[34] S.-S. Diop, L. Fritz, M. Vojta, and S. Rachel, Impurity bound states as detectors of topological band structures revisited, Phys. Rev. B **101**, 245132 (2020).

[35] F. Mazzola, C. M. Yim, V. Sunko, S. Khim, P. Kushwaha, O. J. Clark, L. Bawden, I. Marković, D. Chakraborti, T. K. Kim, M. Hoesch, A. P. Mackenzie, P. Wahl, and P. D. C. King, Tuneable electron-magnon coupling of ferromagnetic surface states in $PdCoO_2$, npj Quantum Mater. **7**, 20 (2022).